ELSEVIER

Materials Science and Engineering B91–92 (2002) 196–210

MATERIALS SCIENCE & ENGINEERING B

www.elsevier.com/locate/mseb

Contactless surface charge semiconductor characterization

Dieter K. Schroder *

Department of Electrical Engineering, Center for Solid State Electronics Research, Arizona State University, Tempe, AZ 85287-5706, USA

Abstract

Surface voltage and surface photovoltage measurements have become important semiconductor characterization techniques, largely because of their contactless nature and the availability of commercial equipment. The use of these contactless measurement techniques has broadened from initial application of minority carrier diffusion length measurements to a wide variety of semiconductor characterization, including surface voltage, surface barrier height, flatband voltage, oxide thickness, oxide charge density, interface trap density, mobile charge density, oxide integrity, generation lifetime, recombination lifetime and doping density. It is likely that this range of applications will broaden further. As with all characterization techniques, there are limitations but they are frequently compensated by the contactless nature of the measurement thereby simplifying test structure fabrication. © 2002 Elsevier Science B.V. All rights reserved.

Keywords: Silicon; Electrical measurements; Metal–insulator–semiconductor structures; Surface and interface states; Contact potential; Work function; Epitaxial silicon

1. Introduction

Test structures are very important during the development of integrated circuits (ICs) and for manufacturing control. To be effective, such test structures should provide rapid feedback to the pilot or manufacturing line. Surface voltage (SV) and surface photovoltage (SPV) semiconductor characterization techniques lend themselves to such rapid feedback test structures. For this reason, they have become powerful and convenient methods for a variety of material/device parameter measurements [1]. The range of the basic technique has been expanded through the addition of corona charge deposited on the sample, illustrated in Fig. 1. The method is particularly attractive because it is usually contactless. The introduction of commercial equipment led to widespread adoption by the semiconductor industry for initially measuring the minority carrier diffusion length. The application base was later expanded to encompass routine characterization of surface voltage, surface barrier height, flatband voltage, oxide thickness, oxide leakage current, interface trap density, mobile charge density, oxide integrity, generation lifetime, recombination lifetime, and doping density. The contactless nature of the measurements, allows for easy contour mapping of a given material/device parameter.

Charge, in these measurements, is used in two basic ways: as the ‘gate’ in MOS-type measurements, where the charge replaces the metal or poly-silicon gate, and as a surface modifying method, where the charge controls the surface potential. In the surface charge/contactless probe technique the probe voltage is measured as a function of time or wavelength to determine the lifetime or diffusion length or the charge is measured as a function of probe voltage to determine oxide properties, e.g. oxide charge, oxide thickness, interface trapped charge, etc. The charge-based approach has an advantage over voltage-based measurements. I will illustrate that with an example. In any measurement, there is a certain amount of uncertainty in the instrumentation. Suppose we want to determine the oxide charge of a MOS device. We can measure the charge or the voltage. The relationship between the oxide voltage uncertainty ΔV_{ox} and the oxide charge uncertainty ΔQ_{ox} is

$$\Delta Q_{ox} = C_{ox}\Delta V_{ox} = K_{ox}\varepsilon_o \Delta V_{ox}/t_{ox} \tag{1}$$

where t_{ox} is the oxide thickness and the other symbols have their usual meaning. Eq. (1) is plotted in Fig. 2.

* Tel.: +480-965-6621; fax: +480-965-8118.
E-mail address: schroder@asu.edu (D.K. Schroder).

0921-5107/02/$ - see front matter © 2002 Elsevier Science B.V. All rights reserved.
PII: S0921-5107(01)00993-X

For $\Delta V_{ox} = 1$ mV, for example, the figure shows ΔQ_{ox} to be oxide thickness dependent, varying from 2.2×10^{10} to 2.2×10^{11} cm^{-2} as the oxide thickness changes from 10 to 1 nm. In other words, if we use voltage-based measurements, there is a large uncertainty in oxide charge. If we make charge-based measurements, there is, of course, a charge uncertainty, but that is independent of oxide thickness and is typically on the order of 10^9 cm^{-2} or less.

In this paper I will give a brief historical perspective, followed by the basic theory of the various methods, and end with some of the more common applications.

2. A brief history

Many of today's recombination lifetime/minority carrier diffusion length characterization tools use corona charge to augment the measurement. The development of these tools had to await the discovery and development of two separate concepts: surface photovoltage and corona charge. Although the concept of surface photovoltage was known in 1953 when it was used during the early days of transistor development at Bell Laboratories [2], it was not until the 1970s that the method was implemented in a practical way in the semiconductor industry at RCA Laboratories. The fundamental theory had been developed earlier. Moss considered diffusion of photo-generated carriers during surface photovoltage measurements in 1955 [3]. He called it 'photovoltage' and the 'photovoltaic effect'. The name 'surface photovoltage' appears to have been used first by Brattain and Garret in 1956 using continuous illumination [4]. Morrison used a chopped light signal for capacitive detection of the voltage [5]. The application of SPV to determine the minority carrier diffusion length was proposed by Moss in 1955, by Johnson in 1957 [6], and by Quillier and Gosar in 1960 [7].

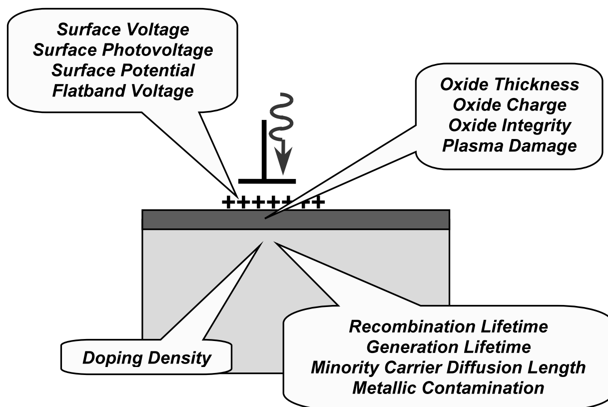

Fig. 1. Schematic illustration of the various material/device parameters measurable with charge/probe techniques.

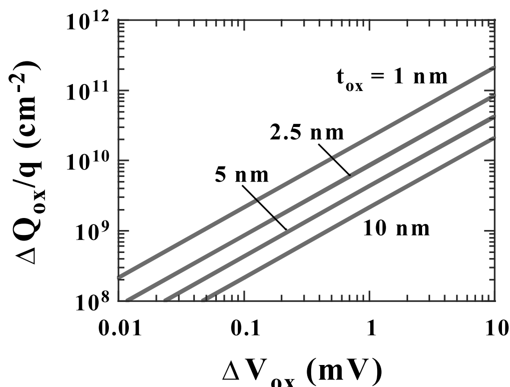

Fig. 2. Oxide charge density uncertainty versus oxide voltage uncertainty as a function of oxide thickness.

Goodman at RCA Laboratories described the method in 1961 in some detail[8] and built an SPV system that was employed during semiconductor production at RCA. It was implemented to characterize the furnace cleanliness by inserting high lifetime wafers into critical furnaces and measuring the diffusion length after heating the wafers [9]. Through this relatively simple, contactless method, they were able to determine cracked furnace tubes, contaminated solid diffusion sources, metallic contamination, and other contamination sources. Jastrzebski cites many examples of the usefulness of the SPV method in the semiconductor industry [10]. Lagowski and Jastrzebski commercialized the SPV system in 1988 when they founded Semiconductor Diagnostics Inc. and introduced a tool to measure minority carrier diffusion lengths in an automated manner. It quickly became very popular in the semiconductor industry, which was heavily dominated by MOS technology. Why? After all, MOSFETs are unipolar devices in which recombination is essentially nonexistent and carrier lifetimes and minority carrier diffusion lengths play almost no role. The key to this wide acceptance was the discovery that iron in boron-doped silicon could be easily determined with minority carrier diffusion length measurements [11,12], using the Fe–B pair to interstitial iron dissociation [13,14]. The fortuitous coupling of the dominant boron-doped silicon starting material for MOS ICs with the ubiquitous iron contaminants, made SPV the ideal tool for diffusion length measurements as process cleanliness monitors.

The commercial implementation of corona charging is relatively new in the semiconductor industry, although it is the basis of copying processes using xerographic techniques [15]. Williams, Willis, Weinberg and Woods from RCA Laboratories, pioneered the application of corona charge to semiconductor characterization [16–18]. They adapted corona charging to selected semiconductor parameter characterization. Verkuil and Fung implemented it as a more complete semiconductor characterization tool at IBM, where new applica-

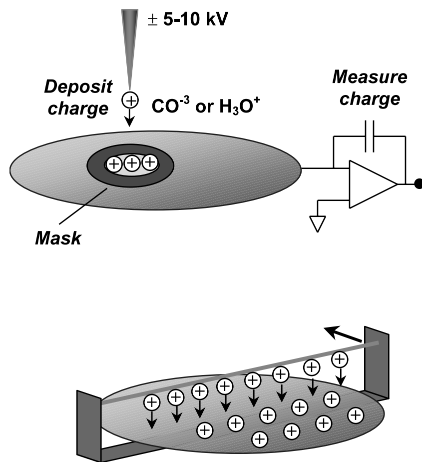

Fig. 3. Schematic illustration of point and wire electrode corona charging methods. The deposited charge is precisely measured with the op-amp charge meter.

tions were developed [19,20]. The IBM technology was subsequently acquired by Keithley Instruments, Inc. and turned into a commercial tool. The technology was then acquired by KLA-Tencor Corp [21]. Corona charge was also incorporated into SPV tools by Semiconductor Diagnostics [22] and into recombination lifetime/diffusion length characterization tools by Semilab [23] and surface charge based measurements by QC Solutions [24].

3. Surface charging

Contactless surface charge characterization requires two key components: a surface charge and a means of determining semiconductor material or device parameters. The semiconductor surface is charged by chemical means or through corona charge deposition. Chemical treatment is as simple as rinsing the sample in water. For surface photovoltage measurements, one requires a depleted surface. For n-type silicon, the oxide on the sample surface should be removed and then the sample should be boiled in H_2O_2 or in water for about 15 min and then rinsed in deionized water (DI) [25]. Alternately, one can soak the sample in $KMnO_4$ for 1–2 min and then rinse it in DI water. These treatments produce a stable depleted surface. For p-type silicon very little treatment is required. In case of very low surface photovoltage, V_{SPV}, etching in buffered HF followed by a DI water rinse is recommended. Other treatments result in other surface conditions. For example, the surface Fermi level has been reported to be close to the valence band for chemical-mechanically polished Si wafers [26]. A dilute rinse in HF/H_2O followed by a water rinse yields positive surface charge [27], as does HNO_3 followed by water and $NH_4OH/H_2O_2/H_2O$ followed by water [28]. In other cases the surface has been treated in an iodine-ethanol solution to reduce surface recombination [29,30].

Corona charging is a second method of depositing charge on a surface. The method consists of depositing ions on a surface at atmospheric pressure through a potential applied to a wire, a series of wires, a single point, or multiple points located a few mm or cm above the sample surface shown in Fig. 3 [31]. A potential of 5000–10,000 V of either polarity is applied to the corona source. For a negative source potential, positive ions bombard the source while ambient molecules rapidly capture free electrons to form negative ions. For a positive source potential, electrons are attracted to the source and positive ions follow the electric field lines to the substrate. The negative and positive corona ionic species are predominantly CO^{-3} and H_3O^+ (hydrated protons), respectively. The corona source forces a uniform flow of ionized air molecules toward the surface. The very short (approximately 0.1 μm) atmospheric mean free path of the ionized gas ensures collision-dominated ion transport with the molecules retaining very little kinetic energy. The charge is not permanent and can be removed by a water rinse or neutralized by charge of opposite polarity.

Another technique to create the effect of deposited charge is the application of a potential between an electrode held above the sample and the sample [28,32], The resulting electric field accumulates, depletes, or inverts the surface, depending on the voltage polarity and magnitude.

4. Theory

A charge gives rise to an electric field, according to Gauss' law

$$\varepsilon = Q/K\varepsilon_o \quad (2)$$

where ε is the electric field, Q the charge/unit area, K the dielectric constant, and ε_o the permittivity of free space. This electric field is most commonly measured with a contactless probe located above the sample. Kelvin first proposed such a probe, usually called a Kelvin probe, in 1881 [33]. Kronik and Shapira give an excellent discussion of such probes and their applications [34]. The probe is a small plate, 2–4 mm in diameter, held above the sample at a distance of typically 0.1–1 mm and vibrated at frequencies of typically 500–600 Hz for signal-to-noise enhancement through lock-in techniques. The required ac signal is obtained by either vibrating the probe, holding the excitation source constant, or holding the probe stationary with an ac excitation source, e.g. modulated light. Two types of probes are used as illustrated in Fig. 4. In the Kelvin probe, the electrode is vibrated vertically changing the capacitance between probe and sample. In the Monroe

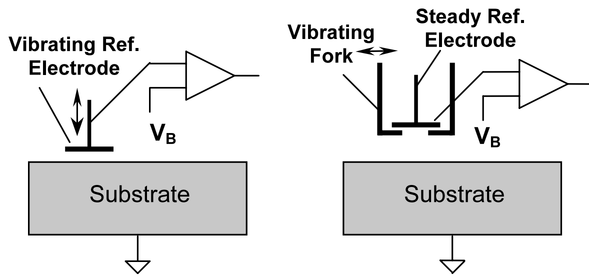

Fig. 4. Kelvin probe (left) and Monroe probe (right) for contact potential difference measurements.

probe, the electrode is fixed and a grounded shutter, mounted in front of the electrode, is vibrated horizontally thereby modulating the probe to wafer capacitance. The difference in design makes Monroe probes less sensitive to external vibrations and the measurement setup need not be vibration isolated.

The energy or potential band diagram of the probe–air–semiconductor system is shown in Fig. 5. W_M and W_S are the metal and semiconductor work function potentials, i.e. potentials between the vacuum potential E_{vac}/q and the Fermi potential ϕ_F. E_c/q and E_v/q are the conduction and valence band potentials. The potential of the intrinsic energy level in the neutral bulk semiconductor, ϕ, is taken as the reference potential. The semiconductor surface potential ϕ_s (ϕ at $x = 0$) is zero for flatband, positive for depletion and inversion, and negative for accumulation for p-type semiconductors.

The potential on the sample surface is the surface voltage V_S. For a bare sample $V_S = \phi_s$, but for an oxidized wafer with charge in or on the oxide, $V_S \neq \phi_s$. The potential measured at the probe is the contact potential difference also called the contact potential, which I denote as the probe potential V_P. All potentials are measured with respect to the grounded substrate. The probe potential, V_p, between the probe and the sample, is determined by measuring the ac current [35]

$$I = V_p \mathrm{d}C/\mathrm{d}t \quad (3)$$

where C is the capacitance between the probe and the sample. The contact potential difference is determined by either calibrating the current versus the bias voltage V_B (Fig. 4), or by adjusting V_B until the current is zero in which case $V_B = V_p$. The former method is faster and is used during wafer mapping.

First consider the bare, grounded p-type semiconductor in Fig. 5 with the metal probe a distance t above the sample. The external nulling voltage V_B ensures zero probe current and zero probe charge. There is no surface charge and W_M and W_S are equal in Fig. 5(a), leading to zero work function difference, i.e. $W_{MS} = W_M - W_S = 0$. Later we will relax this simplification. The band diagram is very similar to that of a MOS capacitor, with the oxide replaced by air. Next, positive charge density Q (C cm^{-2}) is deposited on the semiconductor surface as in Fig. 5(b), inducing equal but opposite polarity charge density Q_S in the semiconduc-

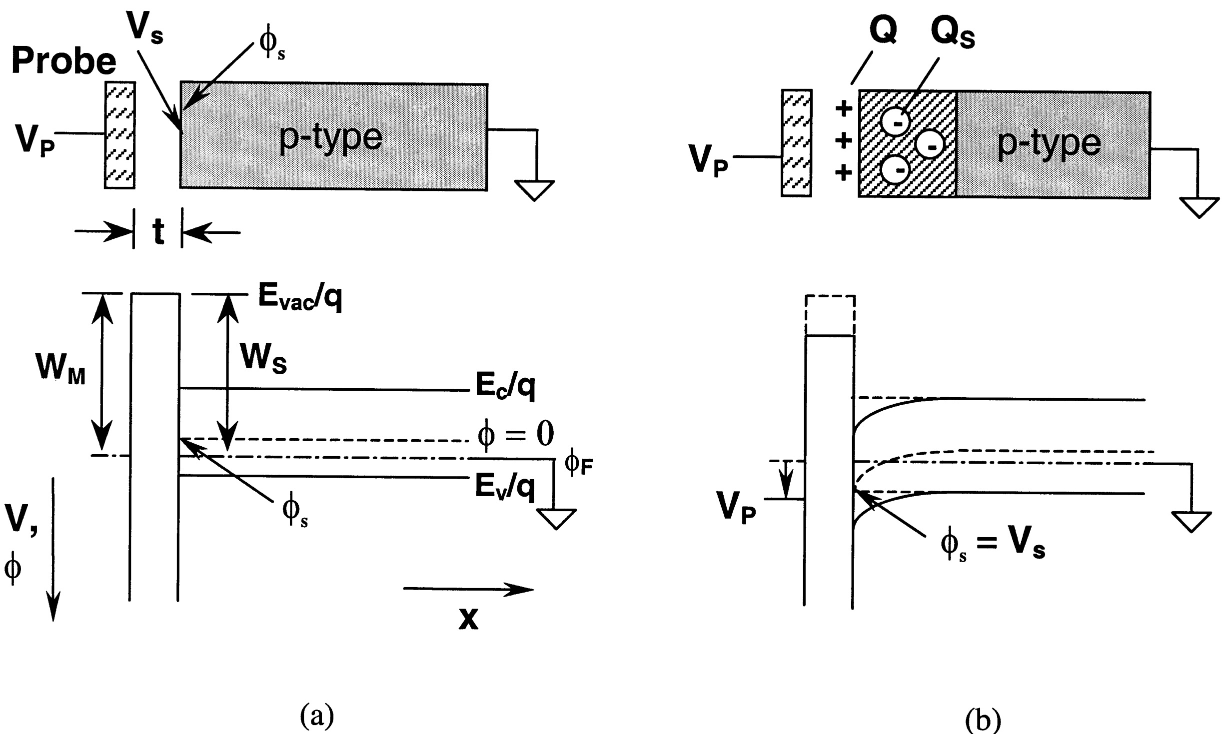

Fig. 5. Cross-section and band diagram of a metal–air–semiconductor system with zero work function difference: (a) no surface charge; (b) with surface charge.

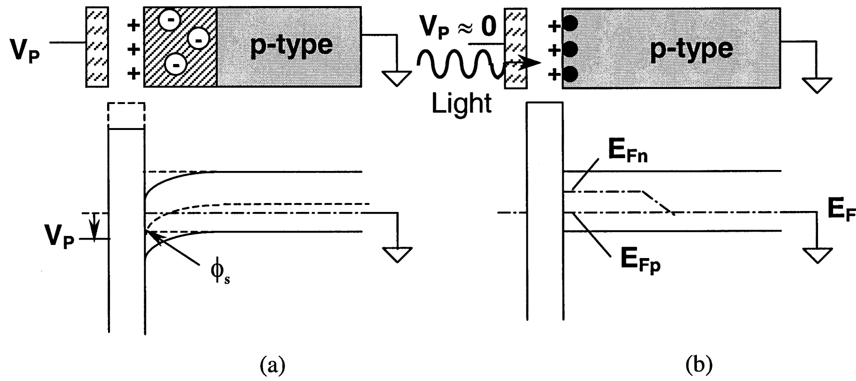

Fig. 6. (a) Band diagram with surface charge in the dark, (b) band diagram with surface charge and strong illumination. The black circles represent electrons.

tor. The dashed lines on the energy band diagram obtain for zero charge and the solid lines for charge density Q, inducing charge only in the semiconductor, not in the nulled probe. Hence, no electric field exists between the sample and the probe making $V_P = V_S = \phi_s$.

The induced semiconductor charge density Q_S, for a depleted surface, consists of ionized acceptors in the space-charge region (scr)

$$Q_S = -qN_A W; \qquad W = \frac{Q}{qN_A} = \sqrt{\frac{2K_s\varepsilon_o\phi_s}{qN_A}} \tag{4}$$

where W is the scr width and N_A the acceptor density. The surface potential ϕ_s becomes

$$\phi_s = \frac{Q^2}{2K_s\varepsilon_o qN_A} = \frac{(qN)^2}{2K_s\varepsilon_o qN_A} = 9.07 \times 10^{-7}\frac{N^2}{K_s N_A} \tag{5}$$

where N is the surface charge atom density (cm^{-2}). The surface potential $\phi_s = 0.077$ V for Si with $N_A = 10^{16}$ cm^{-3}, $K_s = 11.7$ and $N = 10^{11}$ cm^{-2}.

Next we will consider the effect of light on the sample. Fig. 6(a) shows the band diagram in the dark (dashed lines without charge, solid lines with surface charge) and in Fig. 6(b) the sample is strongly illuminated driving it to flatband or near-flatband. Hence, by measuring the surface voltage without and with light, we obtain the surface potential and hence the charge density from Eq. (5). To understand how this comes about, we must look at the flatband condition in more detail.

The semiconductor charge density Q_S for a p-type semiconductor in depletion or inversion is given by

$$Q_S = -\sqrt{2kTK_s\varepsilon_o n_i}F \tag{6}$$

where F is the normalized surface electric field, defined as [36]

$$F = \sqrt{\frac{(p_o/n_i)(e^{-U_S} + U_S - 1) + (n_i/p_o)(e^{U_S} - U_S - 1) + (p_o/n_i)}{(e^{U_S} + e^{-U_S} - 2)(\Delta n/p_o)}} \tag{7}$$

where p_o is the majority carrier density, n_i the intrinsic carrier density, $U_s = q\phi_s/kT$ is the normalized surface potential and $\Delta p = \Delta n$ is the light-generated excess carrier density.

F is plotted versus ϕ_s in Fig. 7 as a function of the normalized excess carrier density. From Gauss' law we know that constant charge corresponds to constant electric field or constant F. Hence as Δn increases, the surface potential decreases, because the locus of the F–ϕ_s plot is along a horizontal line such as the dashed line. It is obvious from Fig. 7 that the surface potential decreases with increasing light-generated excess carriers. In the limit of intense illumination, $\phi_s \to 0$ and the semiconductor approaches flatband, as shown in Fig. 6(b). In other words, a measure of the probe voltage in the dark and under intense light leads to the surface potential according to

$$V_{p,dark} - V_{p,light} = \Delta V_p \approx \phi_s \tag{8}$$

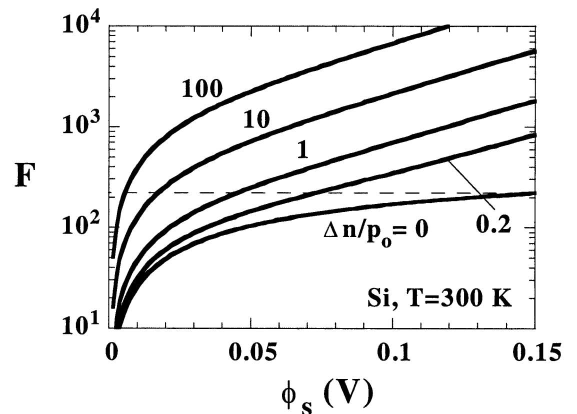

Fig. 7. Normalized surface electric field, F, function vs. surface potential as a function of normalized excess carrier density or light intensity.

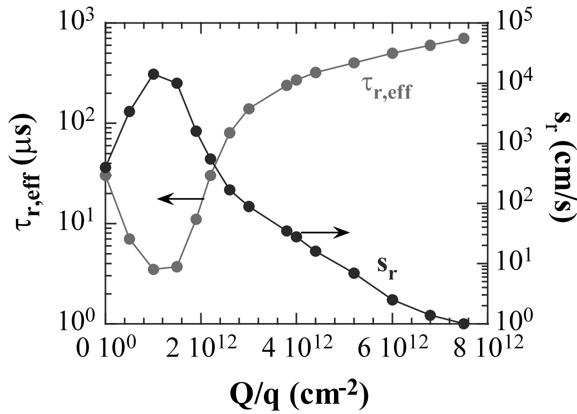

Fig. 8. Effective recombination lifetime and surface recombination velocity as a function of negative surface corona density. $N_A = 4.2 \times 10^{16}$ cm^{-3}, $t = 280$ μm. Data from Ref. [39].

5. Applications

5.1. Carrier lifetime

Carrier lifetime is one of few parameters giving information about the low defect densities in today's ICs. What other technique can detect defect densities as low as 10^{10}–10^{11} cm^{-3} in a simple room temperature measurement? In contrast to analytical techniques whose signals are usually proportional to impurity density, lifetime and diffusion length are inversely proportional to impurity density. Hence, while analytical technique signals decrease, lifetime/diffusion length signals increase with decreasing impurity density. Further, the availability of commercial, clean room compatible equipment makes these measurements relatively simple. It is for these reasons that the IC community has embraced lifetime measurements as a 'process cleanliness monitor'.

Lifetimes are divided into recombination lifetime and generation lifetime [37]. Excess carriers decaying by recombination are characterized by the recombination lifetime, τ_r. Generation lifetime, τ_g, applies when there is a paucity of carriers, as in the space-charge region of a reverse-biased diode or MOS device and the device tries to attain equilibrium through electron-hole pair (ehp) generation. During recombination an electron-hole pair ceases to exist on average after a time τ_r. The generation lifetime, by analogy, is the time that it takes on average to generate an electron-hole pair.

The different types of lifetimes sample different regions of a semiconductor wafer. Creating excess electron-hole pairs and measuring their subsequent recombination yields the recombination lifetime. Excess electron-hole pairs exist typically over a distance of the minority carrier diffusion length, which is on the order of hundreds of microns in Si. For very high quality Si wafers, the diffusion lengths are as high as 2000 μm. Such high lifetime material is difficult to characterize, because surface recombination plays an important, sometimes-dominant role, during the measurement. This is especially serious for epitaxial layers that are typically only a few microns thick. Hence, surface recombination control is very important.

Generation lifetime measurements, on the other hand, lend themselves to characterization of thin layers, because the generation of ehp is measured in a reverse-biased space-charge region. The scr width is controlled through an applied voltage or charge.

When these recombination and generation events occur in the bulk, they are characterized by τ_r and τ_g. When they occur at the surface, they are characterized by the surface recombination velocity s_r and the surface generation velocity s_g. Since devices consist of bulk regions and surfaces, both bulk and surface recombination or generation occur simultaneously and their separation is sometimes quite difficult. Some methods allow this separation while others do not. The measured lifetimes are always effective lifetimes consisting of bulk and surface components.

What role does surface recombination play during lifetime measurements? The effective recombination lifetime, $\tau_{r,eff}$, is a combination of bulk lifetime, τ_B, and surface lifetime, τ_S [38]

$$\frac{1}{\tau_{r,eff}} = \frac{1}{\tau_B} + \frac{1}{\tau_S} \tag{9}$$

The bulk lifetime is inversely proportional to bulk defects and impurities and the surface lifetime is inversely proportional to surface and interface states. Both recombination and generation lifetime measurements can be implemented with corona charge techniques. Let us illustrate this with some examples.

Surface charge, chemical or corona, is used in several modes during lifetime characterization. For example, surface charge can be used to control the surface potential and can lead to low surface recombination by driving the sample into accumulation, depletion, or inversion. This is illustrated in Fig. 8 where the effective lifetime and surface recombination velocity are plotted as a function of surface charge density [39]. The effective lifetime is measured with the photoconductance decay/microwave reflectivity technique [40]. The wafer surface is slightly inverted for zero surface charge. As negative corona charge is deposited, the surface initially depletes. The effective lifetime decreases and the surface recombination velocity increases. As more negative corona charge is deposited, the surface becomes accumulated, surface recombination is suppressed and the lifetime increases. In this case, corona charge was used to modify the surface recombination velocity by controlling the surface condition.

In another approach, the recombination lifetime is determined by depositing charge onto an oxidized

wafer to invert the semiconductor surface forming a field-induced np junction in a p-type substrate, shown in Fig. 9. A brief light pulse injects excess carriers into the sample thereby forward biasing this np junction. The junction bias changes as ehps recombine, leading to a time-dependent probe voltage. This method is very similar to the open-circuit voltage decay technique. The recombination lifetime is determined from the equation [41]

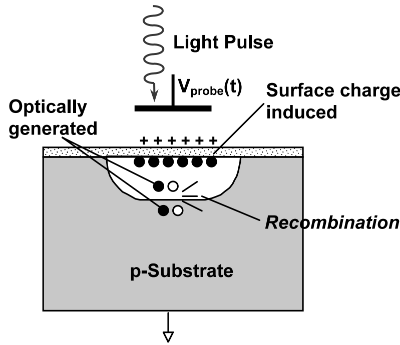

Fig. 9. Corona charge forms a charge-induced np junction. Pulsed light modifies the junction voltage measured with the contactless probe.

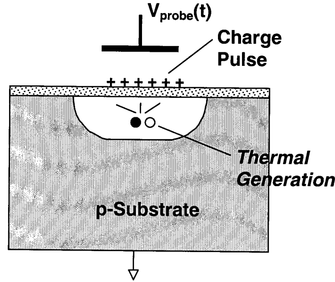

Fig. 10. Corona charge pulse forms a deep-depleted space-charge region. Thermal electron-hole pair generation leads to time varying probe voltage.

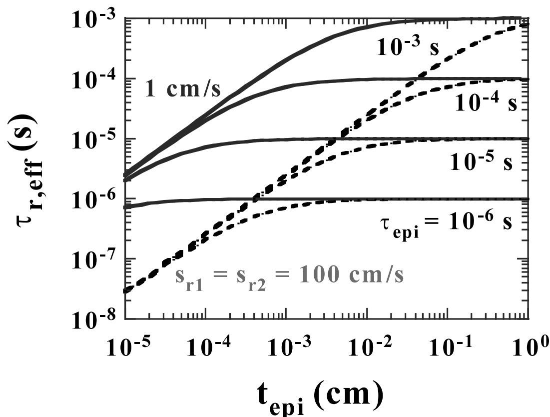

Fig. 11. Effective recombination lifetime versus epitaxial layer thickness as a function of epitaxial layer lifetime.

$$\tau_r = \frac{kT/q}{dV_P/dt} \quad (10)$$

The generation lifetime is determined by depositing a charge pulse onto an oxidized wafer, driving the corona-oxide-semiconductor (COS) device into deep depletion, illustrated in Fig. 10. The wafer is then quickly transported under a Kelvin probe and the probe voltage is measured as a function of time. The space-charge region width is controlled by the amount of corona charge. Electron-hole pairs are subsequently thermally generated and the resulting voltage transient is monitored. The generation lifetime is extracted from the probe voltage transient through the expression [42]

$$\frac{dV_P}{dt} = \frac{qn_i}{C_{ox}}\left(\frac{(W - W_{min})}{\tau_{geff}} - s_{geff}\right) \quad (11)$$

It is difficult to characterize lightly doped epitaxial layers on heavily doped substrates with recombination lifetime or minority carrier diffusion length measurements because the layers are usually much thinner than the minority carrier diffusion length. Excess carriers recombine at the surface, in the epi layer itself, at the epi-substrate interface, and in the substrate. The resultant effective lifetimes are strongly influenced by recombination at the surface and at the epi/substrate interface. Even if the surface is oxidized to reduce surface recombination, the Si/SiO_2 interface can still be a strong contributor to the effective lifetime. To illustrate the effect of surface/interface recombination on the recombination properties, the effective lifetime is plotted versus epi layer thickness as a function of the epi lifetime, τ_{epi}, the surface recombination velocities s_{r1} and s_{r2} at the surface and the epi/substrate interface in Fig. 11. For typical epi layer thicknesses of 10^{-4}–10^{-3} cm, the effective lifetimes are largely dominated by interfacial recombination for lifetimes of 10 μs or higher. Fig. 11 shows that in order to be able to say anything about the epi layer lifetime, the surface recombination velocity has to be very low. Such low s_r can be achieved through effective chemical surface passivation or by driving the surface into accumulation with corona charge.

The epitaxial layer can be characterized through τ_g measurements, however, with the thermal carrier generation confined to the space-charge region, which is typically on the order of 1 μm. Generation and recombination lifetime measurements were recently used to characterize epitaxial films on lightly doped substrates as illustrated in Fig. 12 [43]. The figure shows the results for both 'good' and 'bad' epi-layers and 'good' and 'bad' substrates (SS). There is roughly a factor of ten difference between 'good' and 'bad' generation and recombination lifetimes. This is an excellent example showing how these two complementary techniques yield information that neither one alone can provide.

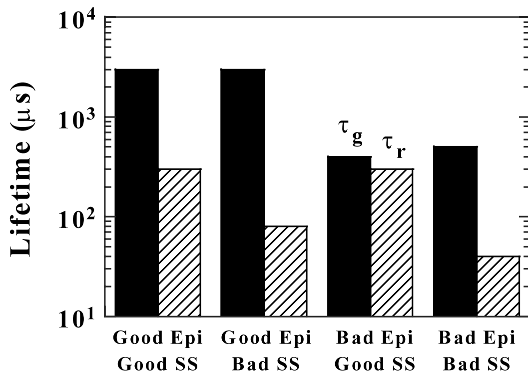

Fig. 12. Corona-induced generation and recombination lifetimes of n-epitaxial layers on n-substrates. Data from Ref. [43].

5.2. Minority carrier diffusion length

The minority carrier diffusion length is related to the recombination lifetime through the relationship

$$L_n = \sqrt{D_n \tau_r} \tag{12}$$

where D_n is the minority carrier diffusion coefficient. The diffusion length is most commonly determined with the surface photovoltage technique. It is a nondestructive and contactless steady-state method, with simple sample preparation (no contacts, junctions, or high temperature processing required), and the equipment is commercially available. The concept of surface photovoltage can be understood with the band diagram in Fig. 13. Surface charge density Q induces an equivalent charge density in the semiconductor, Q_S, in Fig. 13(a). The band diagram in the dark is shown in Fig. 13(b). With illumination, the Fermi level splits into the quasi-Fermi levels E_{Fn} and E_{Fp} with the surface photovoltage equal to the splitting potential as in Fig. 13(c). The light is chopped to enhance the signal/noise ratio using lock-in techniques. The wavelength is varied with a monochromator or a series of filters transmitting selected wavelengths.

Electron-hole pairs are generated by absorbed photons in both the space-charge region and in the p-substrate. Those minority carriers in the quasi-neutral substrate, within approximately a minority carrier diffusion length of the scr edge, diffuse and drift toward the surface, establishing a surface photovoltage relative to the grounded back surface. The surface photovoltage is proportional to the excess minority carrier density, $\Delta n(W)$. The excess carrier density at $x = W$, the scr edge, is related to the surface voltage by the 'law of the junction' from pn junction theory

$$\Delta n(W) = n_o(\exp(qV_S/kT) - 1) \approx n_o qV_S/kT \tag{13}$$

for $V_S \ll kT/q$. The surface voltage is equal to the probe voltage, giving

$$V_P = \frac{kT}{q}\frac{(1-R)\Phi}{n_o(s_1 + D_n/L_n)}\frac{L_n}{(L_n + 1/\alpha)} \tag{14}$$

where Φ is the photon flux density, R the reflectivity, n_o the equilibrium minority carrier density, s_1 the effective surface recombination velocity, D_n the minority carrier diffusion constant, and α the optical absorption coefficient. Typical surface photovoltages are in the low millivolt range, ensuring a linear relationship.

In the constant photon flux density method, the photon flux density is held constant [12]. A series of different wavelengths is selected during the measurement with each wavelength providing a different α. The surface photovoltage is adjusted for each wavelength to hold Φ constant, allowing Eq. (14) to be written as

$$\frac{1}{V_P} = \frac{n_o(s_1 + D_n/L_n)}{(kT/q)(1-R)\Phi}\frac{(L_n + 1/\alpha)}{L_n} = C_1(L_n + 1/\alpha) \tag{15}$$

where C_1 is a constant. A plot of $1/V_P$ versus $1/\alpha$ gives L_n as the intercept.

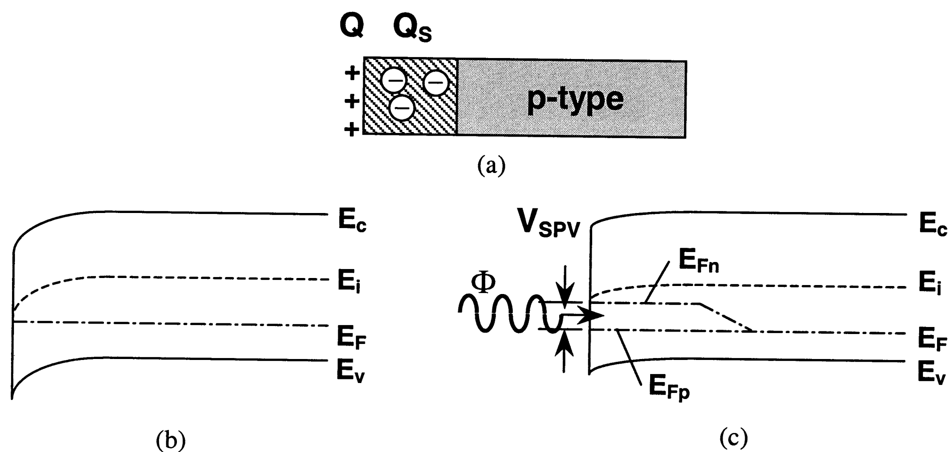

Fig. 13. (a) Device cross section showing the surface charge density Q and the semiconductor charge density Q_S, (b) band diagram in the dark and (c) illuminated band diagram.

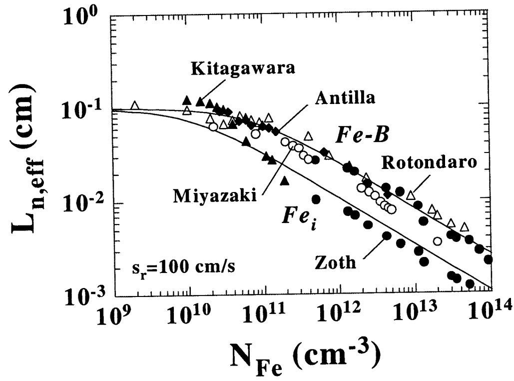

Fig. 14. Effective diffusion lengths versus iron density for Fe–B and Fe_i. s_r is the surface recombination velocity for the theoretical curves (lines). Data (points) from Ref. [46–50].

5.3. Iron in silicon

Iron is one of the most ubiquitous metallic contaminants in silicon with unique properties in p-type silicon, forming Fe–B pairs in boron-doped Si. Upon heating at 150–200 °C for a few minutes or illuminating the device (20 W cm^{-2} halogen light source for about 20 s) [44] the Fe–B pairs dissociate into interstitial iron (Fe_i) and substitutional boron (B_s). The recombination properties of Fe_i differ from those of Fe–B. By measuring the diffusion length before (L_{ni}) and after (L_{nf}) Fe–B pair dissociation, the iron density N_{Fe} is obtained from the expression [45]

$$N_{Fe} = 1.05 \times 10^{16}\left(\frac{1}{L_{nf}^2} - \frac{1}{L_{ni}^2}\right)\ \mathrm{cm}^{-3} \tag{16}$$

with diffusion lengths in units of μm. The Fe_i and Fe–B diffusion lengths as a function of Fe density are shown in Fig. 14 [46–50]. The saturation of the diffusion lengths at low iron densities is due to surface recombination. Maps of diffusion lengths before and after Fe–B pair dissociation and the resultant Fe density are shown in Fig. 15.

5.4. Oxide charge

Corona charge is usually deposited onto oxidized wafers, with the oxide sufficiently thick that the charge does not leak through the oxide. For thin oxides, e.g. room temperature oxides, charge has to be continuously deposited while it discharges through the oxide to the substrate. Considering the charge-oxide-semiconductor as a COS device, the charge, voltage, and capacitance are related through the expression

$$V = Q/C \tag{17}$$

With the capacitance being constant, it is obvious that the voltage and charge are proportional to each other. This surface voltage dependence on charge lends itself to measurements of charge in the insulator or charge on the wafer. Consider the mobile charge density Q_m (typically Na, K or Li) in the oxide of an oxidized Si wafer [51]. To measure such a mobile charge, first deposit positive corona charge, heat the wafer to a moderate temperature of around 200 °C for a few minutes, driving the mobile charge to the oxide-semiconductor interface, cool the sample and determine the flatband voltage V_{FB1}. Repeat the procedure with a negative corona charge to determine V_{FB2}. Q_m is then determined by the flatband voltage difference through the relation

$$Q_m = C_{ox}(V_{FB2} - V_{FB1}) = C_{ox}\Delta V_{FB} \tag{18}$$

The flatband voltage difference ΔV_{FB} is very low for today's thin gate oxides. For example, the flatband voltage due to oxide charge density Q_{ox} uniformly distributed in the oxide is

$$V_{FB} = -\frac{Q_{ox} t_{ox}}{2K_{ox}\varepsilon_o} \tag{19}$$

For $Q_{ox}/q = 10^{10}$ cm^{-2}, we find $V_{FB} = -2.3 \times 10^3 t_{ox}$ V (t_{ox} in cm). For $t_{ox} = 5$ nm, $V_{FB} = -1.2$ mV, illustrating that such flatband voltage measurements become impractical for thin oxides.

This problem is solved by measuring the surface potential of an oxidized wafer through surface voltage measurements in the dark and with intense light. Then deposit corona charge until the surface potential becomes zero, i.e. semiconductor flatband. By definition, there is no charge in the semiconductor under flatband conditions. The deposited corona charge is then equal in magnitude but opposite in sign to the original oxide charge [52]. The accuracy and precision of this charge-based measurement is independent of oxide thickness. What is lost in this measurement is information about the location of the oxide charge.

The oxide charge is related to the oxide voltage through the relationship $Q_{ox} = C_{ox}V_{ox}$. Considering an uncertainty in the voltage measurement of ΔV_{ox}, leads to a charge uncertainty of

$$\Delta Q_{ox} = C_{ox}\Delta V_{ox} \tag{20}$$

It is obvious that for a given voltage uncertainty, the charge uncertainty is very much dependent on oxide thickness. In charge-based measurements, the charge uncertainty is independent of oxide thickness. A comparison of the two approaches is shown in Fig. 16, where the charge measurement uncertainty has a 3σ variation of 2×10^{10} cm^{-2}. In addition to oxidation-induced charges, one can also measure plasma-induced charge and damage[53,54] and oxide charge in buried oxides of silicon-on-insulator materials [55].

5.5. Oxide thickness, interface state density

The oxide thickness is determined by depositing corona charge density Q on the oxidized wafer and measuring the surface voltage, given by [56]

$$V_S = W_{MS} + V_{ox} + \phi_s \tag{21}$$

With the device biased into accumulation or inversion, the capacitance is equal to the oxide capacitance and the capacitance and oxide thickness are given by

$$C_{ox} = \frac{dQ}{dV_{ox}} \approx \frac{dQ}{dV_S}; \quad t_{ox} = \frac{K_{ox}\varepsilon_o}{C_{ox}} \tag{22}$$

Charge is deposited on the sample surface in precisely measured amounts and the resulting surface voltage is measured with a Kelvin probe. The work function difference W_{MS} is constant, but the semiconductor surface potential ϕ_s changes with charge. As shown earlier, it is possible to determine ϕ_s using strong light. However, ϕ_s is reasonably constant for the device in strong inversion or accumulation. The surface voltage is then

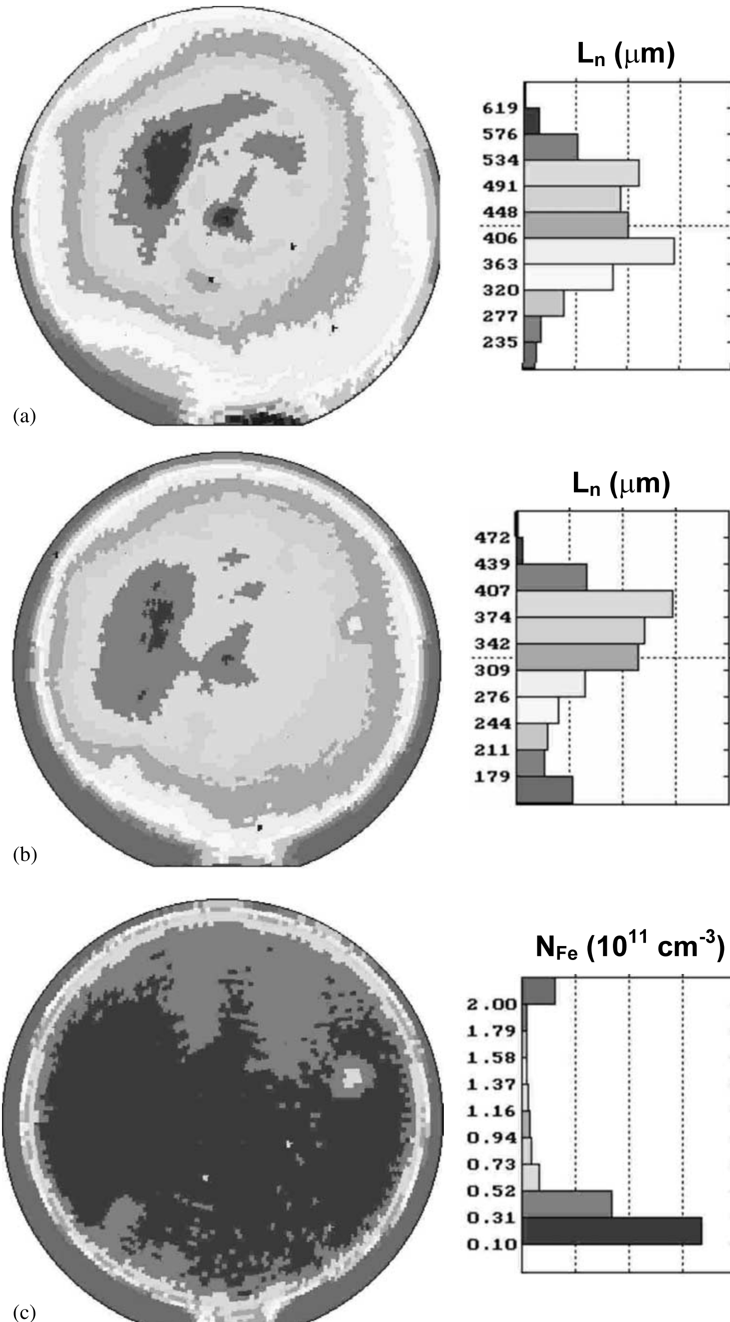

Fig. 15. Diffusion length maps (a) before, (b) after Fe–B pair dissociation, (c) iron density map. Courtesy of P. Edelman and J. Lagowski, Semiconductor Diagnostics, Inc.

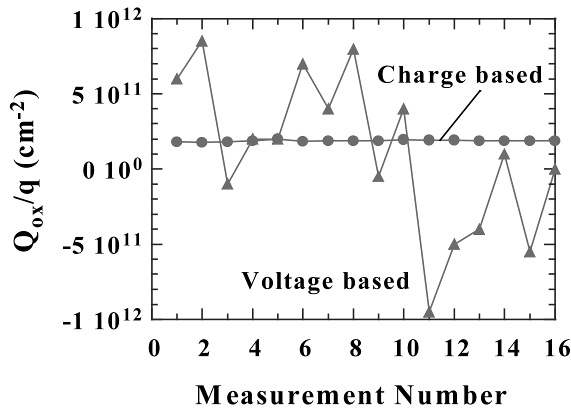

Fig. 16. Charge-based and voltage-based oxide charge repeatability for 3 nm oxides. After Weinzierl and Miller [52].

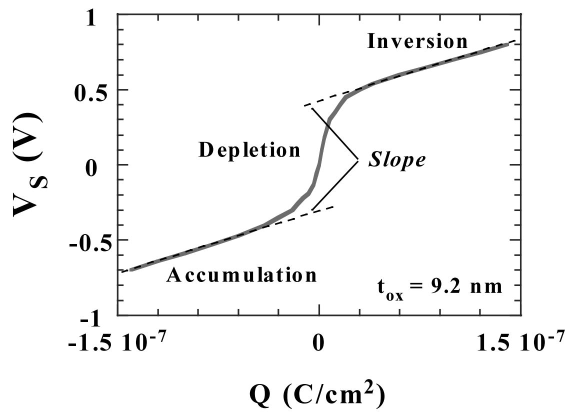

Fig. 17. Surface potential vs. surface charge density showing the various regions of the device. $t_{ox} = 9.2$ nm. After Roy et al. [56].

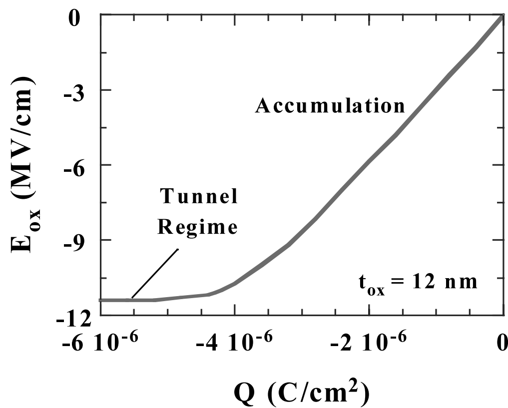

Fig. 18. Oxide electric field vs. surface charge density for an oxidized Si wafer. $t_{ox} = 12$ nm. After Roy et al. [56].

plotted as function of deposited charge density as shown in Fig. 17 and the oxide capacitance is determined from the slope [57]. This method is not subject to the poly-Si gate depletion effects that affect conventional MOS-C measurements [58]. Repeatability of 0.01 nm has been demonstrated for 1.8 nm thick oxides [52].

One of the advantages for oxide thickness and oxide integrity measurements using corona charge 'gates' rather than conductive gates, is the low surface mobility of the surface 'corona' ions. The oxide will, of course, break down at its weakest spot, but the oxide breakdown current is confined to the breakdown spot, because the surface corona charge does not readily drift or diffuse along the surface, making corona charge oxide thickness and oxide breakdown measurements less sensitive to oxide pinholes. By contrast, for conductive gates, the current from the entire gate area will be channeled into the weak spot, frequently leading to catastrophic breakdown.

Fig. 17 shows linear portions of the V_S–Q curve in inversion and accumulation. These regions are used for oxide thickness extraction. The curved depletion region portion of the curve contains information about interface state densities. Just like C–V curves in MOS capacitors are distorted by interface states, so the V_S–Q curve is distorted by interface states and their density can be extracted from this distortion.

5.6. Oxide leakage current

To determine oxide leakage current, usually known as gate current in MOS devices, deposit corona charge on the surface of an oxidized wafer and measure the surface voltage as a function of time. With the device biased into accumulation or inversion, the oxide leakage current is related to the voltage through the relationship [59]

$$I_{leak} = C_{ox}\frac{dV_P}{dt} \Rightarrow V_P(t) = \frac{I_{leak}}{C_{ox}}t \tag{23}$$

There is a limit to the amount of charge that can be deposited on the oxide for this measurement, because the charge density is related to the oxide electric field ε_{ox} through the relationship

$$Q = K_{ox}\varepsilon_o\varepsilon_{ox} \tag{24}$$

As the charge builds up, the surface voltage increases, until the charge density becomes so high that it leaks through the oxide by Fowler–Nordheim or direct tunneling and the surface voltage is clamped. Silicon dioxide breaks down at electric fields of 10–14 MV cm^{-1}. For $\varepsilon_{ox} = 12$ MV cm^{-1}, the 'breakdown' charge is 4.1×10^{-6} C cm^{-2}. Fig. 18 is a plot of ε_{ox} versus Q clearly showing the electric field saturation at a charge density of around 4.4×10^{-6} C cm^{-2}.

6. Frequency-dependent surface photovoltage

Most SPV measurements are made under dc conditions, although the incident light is chopped at a moderate frequency (typically 500–600 Hz) for

signal-to-noise enhancement. However, there is information to be gained from ac-modulated incident light. For example, using frequency-modulated light as the excitation source eliminates the need to vibrate the Kelvin probe. The requirements on the back contact are also relaxed with a suitable capacitive contact.

Nakhmanson originally put forth the theory for frequency-dependent SPV measurements [60,61]. Munakata et al. later implemented it [62,63] with a flying spot scanner incorporating both blue and infrared light sources [64]. The blue light, absorbed near the surface, characterizes the semiconductor near the surface, while the infrared light probes deeper into the wafer. By scanning the light beam, wafer maps can be generated in a few minutes. The surface photovoltage depends on the semiconductor band bending, which depends on the surface charge density. Hence ac SPV measurements lend themselves to surface charge density measurements [65].

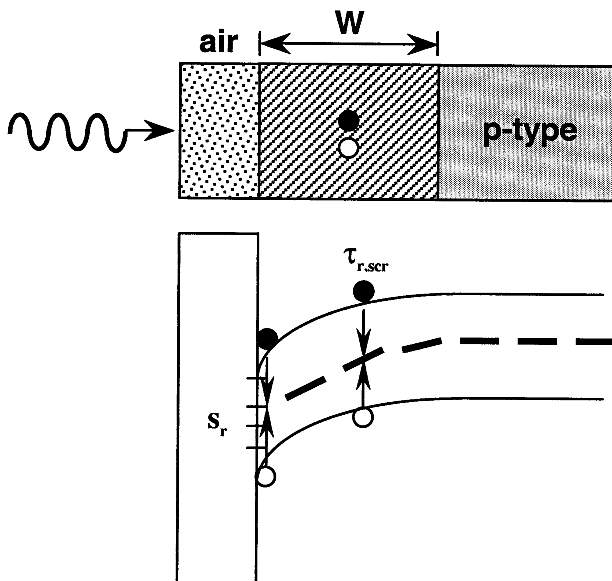

Fig. 19. The sample geometry and recombination of excess carriers in the space-charge region.

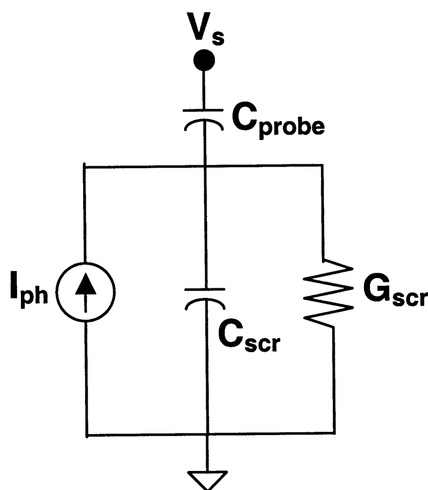

Fig. 20. The equivalent circuit of the SPV measurement system.

In another version of ac SPV, the semiconductor surface is depleted/inverted by chemically induced surface charges and a sinusoidally modulated, low-intensity light generates excess carriers. The carrier lifetime is determined from the ratio of the real and imaginary SPV signals. Short wavelength light ($\lambda = 0.4$ μm) with high absorption coefficient ensures carrier generation near the surface. Hence, the measured lifetime is primarily determined by the oxide-semiconductor interface, i.e. surface recombination, and is sometimes termed the 'surface lifetime' [66]. The signal also contains the substrate doping density or resistivity, leading to contactless resistivity measurements [67].

For ac SPV lifetime characterization, we are considering the sample configuration of Fig. 19. Charge on the surface of the p-type wafer induces a space charge of width W. Incident light generates electron-hole pairs in the sample and the resulting surface photovoltage is measured. Since it is impossible to separate surface and bulk scr recombination with a simple two-terminal measurement, we combine the surface recombination velocity, s_r, and the space-charge region recombination lifetime, $\tau_{r,scr}$, into the effective lifetime τ_{scr}, also known as the near-surface lifetime or the surface-dominated lifetime. In the equivalent circuit of Fig. 20 the monochromatic, ac-modulated light generates the photocurrent I_{ph}. The capacitance C_{scr} represents the semiconductor surface charge-induced space-charge region and C_{probe} is the probe capacitance. The conductance G_{scr} represents the loss mechanism in the semiconductor due to carrier recombination illustrated in Fig. 19.

So far we have been concerned with dc behavior. Since we are ultimately interested in ac excitation, we need to consider the ac behavior of the various lifetimes. Mathematical analyses of steady-state solutions usually assume all pertinent parameters to have an 'exp(jωt)' dependence, with $\omega = 2\pi f$ the radial frequency. A consequence of this modification is that the diffusion length and the lifetime become time-varying functions, defined by [68]

$$L_n = \frac{L_{no}}{\sqrt{1 + j\omega t}}; \qquad \tau = \frac{\tau_o}{1 + j\omega t} \tag{25}$$

where L_{no} and τ_o are the dc values.

In the circuit in Fig. 20, the photocurrent flows primarily through C_{scr} and G_{scr}. The current through C_{probe} can be neglected, because the probe terminal is connected to a high-impedance voltmeter and C_{probe} is a very small capacitance leading to a high impedance. The impedance and phase angle are given by

$$Z = \frac{1}{G_{scr} + j\omega C_{scr}}; \qquad \theta = \tan^{-1}(X/R) \tag{26}$$

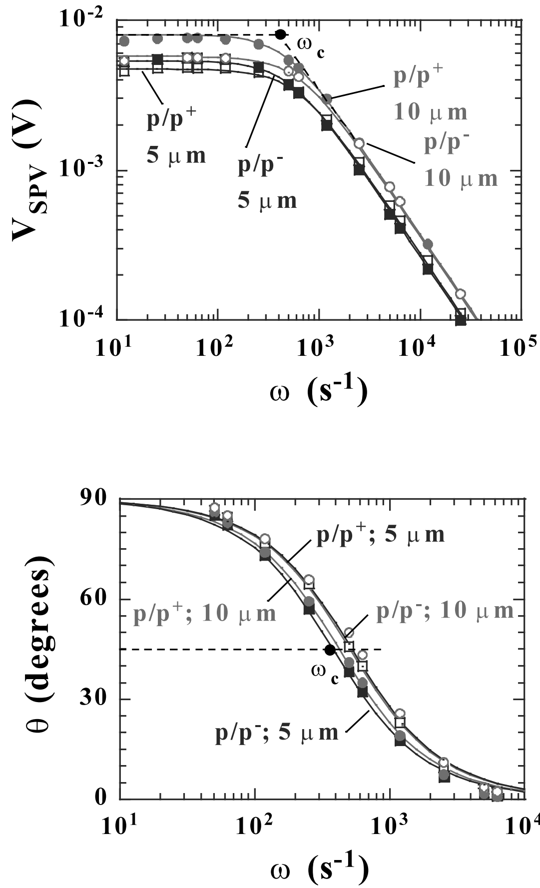

Fig. 21. Surface photovoltage (top) and phase angle (bottom) vs. frequency. τ_{scro}: 1.0–1.3 μs, $\tau_{ro} = 10$ μs, $T = 300$ K. Points: experiment; lines: theory.

where X is the reactance and R the resistance, related to the impedance Z by

$$Z = \sqrt{R^2 + X^2} \tag{27}$$

G_{scr} can be written as [69]

$$G_{scr} = \frac{q^2 n_i W}{\tau_{scr} kT} \tag{28}$$

With $\tau_{scr} = \tau_{scro}/(1 + j\omega\tau_{scro})$ the impedance and phase become

$$Z = \frac{G_{scr}^{-1}}{1 + j\omega C_{scr}/G_{scr}} = \frac{kT\tau_{scro}}{q^2 n_i W(1 + j\omega/\omega_c)};$$

$$\theta = \tan^{-1}(\omega/\omega_c) \tag{29}$$

To extract the lifetime, we determine the corner-frequency, ω_c, given by

$$\omega_c = \frac{1}{\tau_{scro}\left(1 + \dfrac{kTC_{scr}}{q^2 n_i W}\right)} = \frac{1}{\tau_{scro}\left(1 + \dfrac{kTN_A}{2qn_i\phi_s}\right)} \tag{30}$$

The corner frequency depends on the low-frequency scr recombination lifetime, τ_{scro}, the surface potential ϕ_s, the doping density N_A, and n_i. The surface photovoltage is

$$V_{SPV} = J_{ph} Z \tag{31}$$

The ac photovoltage was measured with the Semiconductor Diagnostics Epi Tau FAast 330 system, using a chemically induced surface space-charge region. We characterized epitaxial wafers with two different doping profiles. The p/p^+ sample consists of an epitaxial layer, doped to 10^{15} cm^{-3}, deposited on a highly doped substrate doped to 10^{18} cm^{-3}. The p/p^- sample consists of an epitaxial layer, doped to 10^{15} cm^{-3}, deposited on a moderately doped substrate doped to 10^{15} cm^{-3}. The epitaxial layer thicknesses are 5 and 10 μm for both samples. The light has a wavelength of 400 nm with an absorption coefficient of 2×10^4 cm^{-1}, leading to an absorption depth $1/\alpha = 0.5$ μm with most of the light absorbed in the space-charge region. The lifetime is obtained from the corner frequency expression of Eq. (30), with the corner frequency ω_c obtained from either the surface photovoltage or from the 45° angle of the phase plot.

The effects of substrate doping density and epi layer thickness on V_{SPV} and phase are shown in Fig. 21, where the agreement between experimental data and our theory is excellent in all cases for both surface photovoltage and phase. The space-charge recombination lifetimes and photon flux densities necessary to give this agreement are shown in Table 1. Note that in all cases, the lifetime increases with increasing temperature. The lifetimes of the p/p^+ samples are very similar to those for the p/p^- samples for both thicknesses.

To compare the frequency-dependent method with conventional surface photovoltage diffusion length

Table 1
Sample type, thickness, measurement temperature, near-surface lifetime (measured by the ac technique of this paper), minority carrier diffusion length (measured by conventional SPV), and generation lifetime (measured by pulsed MOS capacitor)

Sample	Thickness (μm)	Temperature (K)	Near-surface lifetime (μs)	Diffusion length (μm)	Generation lifetime (μs)
p/p^+	5	300	1.3	4.5	235
p/p^+	10	300	1.3	7	142
p/p^-	5	300	1.2	330	104
p/p^-	10	300	1.2	304	113

measurements, we measured the diffusion length of both epitaxial wafers (p/p$^+$: $10^{15}/10^{18}$ cm^{-3}; p/p$^-$: $10^{15}/10^{15}$ cm^{-3}). In these measurements, photons with low absorption coefficients are used leading to carrier excitation through the epitaxial layer and a significant portion of the substrate. In that case, it is mainly the thickness of the epitaxial layer that is measured, if the diffusion length of the substrate is significantly lower than that of the p-epi layer, as it would be for the p/p$^+$ samples [70–72]. Our results are shown in Table 1. For the p/p$^+$ samples, the diffusion lengths are indeed approximately equal to the layer thicknesses, while for the p/p$^-$ samples there is no relationship with thickness, as expected.

The ac SPV method is an scr-confined recombination lifetime measurement, because excess carriers are created by light. Another scr-confined measurement is the pulsed MOS capacitor technique, in which the device is pulse-biased into deep depletion and the recovery time of the device due to thermal electron-hole pair generation is measured in the dark leading to the generation lifetime τ_g. We have made such measurements on these wafers, after oxidizing them and depositing poly-Si gates. Generation lifetimes are typically much higher than recombination lifetimes [37]. Table 1 also shows τ_g with values of several hundred μs, much higher than the near-surface lifetimes of around 1 μs.

7. Summary

Surface voltage and surface photovoltage measurements are reviewed here. After a brief history, tracing the technique to 1953, the theory of these techniques is developed. In order for a surface voltage to exist, there must be a charge on the sample. Rinsing the sample in certain solutions or depositing corona charge on it most commonly does this. Rinsing is usually done on bare samples and corona charge is deposited on samples covered by insulators. Corona charge can be deposited on thin, room temperature oxides on silicon, but the charge must be continuously replenished as it leaks through the oxide. The measurement is easier to carry out on thicker oxides. The application of these contactless measurement techniques has broadened from the initial minority carrier diffusion length measurements to a wide variety of semiconductor characterization, including surface voltage, surface barrier height, flatband voltage, oxide thickness, oxide charge density, interface trap density, mobile charge density, oxide integrity, generation lifetime, recombination lifetime, and doping density. It is likely that this range of application will broaden further. As with all characterization techniques, there are limitations and some of these are also discussed. I have chosen to limit my discussion to the necessary concepts augmented with appropriate band diagrams and the necessary equations to explain the measurement and its interpretation.

Acknowledgements

The research leading to this paper was partially funded by the Silicon Wafer Engineering and Defect Science Consortium (SiWEDS) (Intel, Komatsu Electronic Metals, MEMC Electronic Materials, Mitsubishi Silicon, Okmetic, Nippon Steel, SEH America, Sumitomo Sitix Silicon, Texas Instruments, and Wacker Siltronic Corp.).

References

[1] D.K. Schroder, Meas. Sci. Technol. 12 (2001) R16.
[2] W.H. Brattain, J. Bardeen, Bell Syst. Tech. J. 32 (1953) 1.
[3] T.S. Moss, J. Electron. Ctl. 1 (1955) 126.
[4] W.H. Brattain, C.G.B. Garrett, Bell Syst. Tech. J. 35 (1956) 1019.
[5] S.R. Morrison, J. Phys. Chem. 57 (1953) 860.
[6] E.O. Johnson, J. Appl. Phys. 28 (1957) 1349.
[7] A. Quillier, P. Gosar, J. Phys. Rad. 21 (1960) 575.
[8] A.M. Goodman, J. Appl. Phys. 32 (1961) 2550.
[9] A.M. Goodman, L.A. Goodman, H.F. Gossenberger, RCA Rev. 44 (1983) 326.
[10] L. Jastrzebski, in: H.R. Huff, K.G. Barraclough, J. Chikawa (Eds.), Semiconductor Silicon, Electrochemical Society, Pennington, NJ, 1990, p. 614.
[11] G. Zoth, W. Bergholz, J. Appl. Phys. 67 (1990) 6764.
[12] J. Lagowski, P. Edelman, M. Dexter, W. Henley, Semicond. Sci. Technol. 7 (1992) A185.
[13] K. Graff, H. Pieper, J. Electrochem. Soc. 128 (1981) 669.
[14] L.C. Kimerling, J.L. Benton, J.J. Rubin, Inst. Phys. Conf. Ser. 59 (1981) 217.
[15] R.M. Shaffert, Electrophotography, Wiley, New York, 1975.
[16] R. Williams, A. Willis, J. Appl. Phys. 39 (1968) 3731.
[17] R. Williams, M.H. Woods, J. Appl. Phys. 44 (1973) 1026.
[18] Z.A. Weinberg, Solid-State Electron. 20 (1977) 11.
[19] R.L. Verkuil, Abstr. No. 263, Spring Electrochemical Society Meeting, 1981.
[20] R.L. Verkuil, M.S. Fung, Abstr. No. 169, Extended Abstracts 88-1, Electrochemical Society Meeting, 1988, pp. 261–262.
[21] http://www.kla-tencor.com
[22] http://www.sditampa.com
[23] http://www.semilab.com
[24] http://www.qcsolutions.com
[25] Semiconductor Diagnostics Inc. Manual ‘Contamination Monitoring System Based on SPV Diffusion Length Measurements,’ SDI, 1993.
[26] C.A. Sebenne, J.P. Lacharme, I. Andriamanantenasona, M. Khial, Appl. Surf. Sci. 41/42 (1989) 352.
[27] H. Shimizu, C. Munakata, Semicond. Sci. Technol. 5 (1990) 842.
[28] A. Tada, M. Hirano, M. Ichimura, E. Arai, H. Takamatsu, S. Sumie, Jpn. J. Appl. Phys. 40 (2001) 3069.
[29] T.S. Horányi, T. Pavelka, P. Tüttö, Appl. Surf. Sci. 63 (1993) 306.
[30] H. M’saad, J. Michel, J.J. Lappe, L.C. Kimerling, J. Electron. Mater. 23 (1994) 487.
[31] R.B. Comizzoli, J. Electrochem. Soc. 134 (1987) 424.

[32] M. Kohno, S. Hirae, H. Okada, H. Matsubara, I. Nakatani, Y. Imaoka, T. Kusuda, T. Sakai, Jpn. J. Appl. Phys. 35 (1996) 5539.
[33] L. Kelvin, Philos. Mag. 46 (1898) 82.
[34] L. Kronik, Y. Shapira, Surf. Sci. Rep. 37 (1999) 1.
[35] J. Lagowski, P. Edelman, 7th International Conference on Defect Recognition and Image Proc., 1997.
[36] E.O. Johnson, Phys. Rev. 111 (1958) 153.
[37] D.K. Schroder, IEEE Trans. Electron. Dev. ED-29 (1982) 1336.
[38] D.K. Schroder, IEEE Trans. Electron. Dev. 44 (1997) 160.
[39] M. Schöfthaler, R. Brendel, G. Langguth, J.H. Werner, First WCPEC, 1994, p. 1509.
[40] D.K. Schroder, Semiconductor Material and Device Characterization, 2nd ed., Wiley–Interscience, New York, 1998, pp. 429–437.
[41] D.K. Schroder, Semiconductor Material and Device Characterization, 2nd ed., Wiley–Interscience, New York, 1998, pp. 459–463.
[42] D.K. Schroder, M.S. Fung, R.L. Verkuil, S. Pandey, W.H. Howland, M. Kleefstra, Solid-State Electron. 42 (1998) 505.
[43] P. Renaud, A. Walker, Solid State Technol. 43 (2000) 143.
[44] J. Lagowski, P. Edelman, A.M. Kontkiewicz, O. Milic, W. Henley, L. Jastrzebski, A.M. Hoff, Appl. Phys. Lett. 32 (1993) 3043.
[45] G. Zoth, W. Bergholz, J. Appl. Phys. 67 (1990) 6764.
[46] G. Zoth, W. Bergholz, J. Appl. Phys. 67 (1990) 6764.
[47] O.J. Antilla, M.V. Tilli, J. Electrochem. Soc. 139 (1992) 1751.
[48] Y. Kitagawara, T. Yoshida, T. Hamaguchi, T. Takenaka, J. Electrochem. Soc. 142 (1995) 3505.
[49] M. Miyazaki, S. Miyazaki, T. Kitamura, T. Aoki, Y. Nakashima, M. Hourai, T. Shigematsu, Jpn. J. Appl. Phys. 34 (1995) 409.
[50] A.L.P. Rotondaro, T.Q. Hurd, A. Kaniava, J. Vanhellemont, E. Simoen, M.M. Heyns, C. Claeys, J. Electrochem. Soc. 143 (1996) 3014.
[51] D.K. DeBusk, A.M. Hoff, Solid State Technol. 42 (1999) 67.
[52] S.R. Weinzierl, T.G. Miller, in: B.O. Kolbesen, C. Claeys, P. Stallhofer, F. Tardif, J. Benton, T. Shaffner, D. Schroder, S. Kishino, P. Rai-Choudhury (Eds.), Analytical and Diagnostic Techniques for Semiconductor Materials, Devices and Processes, vol. ECS 99-16, Electrochemical Society, Pennington, NJ, 1999, pp. 342–350.
[53] K. Nauka, J. Lagowski, in: D.G. Seiler, A.C. Diebold, W.M. Bullis, T.J. Shaffner, R. McDonald, E.J. Walters (Eds.), Characterization and Metrology for ULSI Technology: 1998 International Conference, American Institute of Physics, 1998, pp. 245–249.
[54] M.S. Fung, Semicond. Int. 20 (1997) 211.
[55] K. Nauka, Microelectron. Eng. 36 (1997) 351.
[56] P.K. Roy, C. Chacon, Y. Ma, I.C. Kizilyalli, G.S. Horner, R.L. Verkuil, T.G. Miller, in: P. Rai-Choudhury, J.L. Benton, D.K. Schroder, T.J. Shaffner (Eds.), Diagnostic Techniques for Semiconductor Materials and Devices, vol. PV97-12, Electrochemical Society, Pennington, NJ, 1997, pp. 280–294.
[57] T.G. Miller, Semicond. Int. 18 (1995) 147.
[58] S.H. Lo, D.A. Buchanan, Y. Taur, IBM J. Res. Dev. 43 (1999) 327.
[59] Z.A. Weinberg, W.C. Johnson, M.A. Lampert, J. Appl. Phys. 47 (1976) 248.
[60] R.S. Nakhmanson, Solid-State Electron. 18 (1975) 617.
[61] R.S. Nakhmanson, Solid-State Electron. 18 (1975) 627.
[62] C. Munakata, S. Nishimatsu, N. Homma, K. Yagi, Jpn. J. Appl. Phys. 11 (1984) 1451.
[63] C. Munakata, S. Nishimatsu, Jpn. J. Appl. Phys. 25 (1986) 807.
[64] K. Kinameri, C. Munakata, K. Mayama, J. Phys. E: Sci. Instrum. 21 (1988) 91.
[65] H. Shimizu, C. Munakata, J. Appl. Phys. 73 (1993) 8336.
[66] E. Kamieniecki, in: D.C. Gupta, F.R. Bacher, W.M. Hughes (Eds.), Recombination Lifetime Measurements in Silicon, vol. STP 1340, ASTM, Philadelphia, PA, 1998, p. 147.
[67] P. Roman, J. Staffa, S. Fakhouri, M. Brubaker, J. Ruzyllo, K. Torek, E. Kamieniecki, J. Appl. Phys. 83 (1998) 2297.
[68] J.P. McKelvey, Solid State and Semiconductor Physics, Harper and Row, New York, 1966.
[69] J.E. Park, D.K. Schroder, S.E. Tan, B.D. Choi, M. Fletcher, A. Buczkowski, F. Kirscht, J. Electrochem. Soc., in press.
[70] J.W. Slotboom, M.J.J. Theunissen, IEEE Electron. Dev. Lett. EDL-4 (1983) 403.
[71] D.K. Schroder, Solid State Electron. 27 (1984) 247.
[72] C.W. Pearce, R.J. Jaccodine, IEEE Trans. Electron. Dev. 38 (1991) 2155.